Mon. Not. R. Astron. Soc. **000**, 1–12 (2002) Printed 24 February 2013 (MN LATEX style file v2.2)

Discovery of a detached H I gas shell surrounding α Orionis

T. Le Bertre[1], L. D. Matthews[2], E. Gérard[3] and Y. Libert[4]
[1] *LERMA, UMR 8112, CNRS & Observatoire de Paris, 61 av. de l'Observatoire, F-75014 Paris, France*
[2] *MIT Haystack Observatory, Off Route 40, Westford, MA 01886, USA*
[3] *GEPI, UMR 8111, CNRS & Observatoire de Paris, 5 place J. Janssen, F-92195 Meudon Cedex, France*
[4] *IRAM, 300 rue de la Piscine, Domaine Universitaire, F-38406 Saint Martin d'Hères, France*

Accepted 2012 March 1. Received 2012 February 24; in original form 2011 December 28

ABSTRACT

We report the detection of the H I line at 21 cm in the direction of α Ori with the Nançay Radiotelescope and with the Very Large Array.

The observations confirm the previous detection of H I emission centered on α Ori, but additionally reveal for the first time a quasi-stationary detached shell of neutral atomic hydrogen $\sim 4'$ in diameter (0.24 pc at a distance of 200 pc). The detached shell appears elongated in a direction opposite to the star's space motion.

A simple model shows that this detached atomic gas shell can result from the collision of the stellar wind from α Ori with the local interstellar medium (ISM). It implies that α Ori has been losing matter at a rate of $\sim 1.2 \times 10^{-6}\,\mathrm{M_\odot\,yr^{-1}}$ for the past 8×10^4 years.

In addition, we report the detection of atomic hydrogen associated with the far-infrared arc located $6'$ north-east of α Ori, that has been suggested to trace the bow shock resulting from the motion of the star through the ISM. We report also the detection by the Galaxy Evolution Explorer (GALEX) of a far-UV counterpart to this arc.

Key words: circumstellar matter – stars: individual: α Ori – supergiants – stars: mass-loss – radio lines: stars.

1 INTRODUCTION

Evolved late-type stars (AGB stars and red supergiants) are observed to undergo mass loss at high rates. They are thus surrounded by expanding circumstellar envelopes (CSEs). Observations show a wide variety of different properties of the central stars and of the CSEs, which are not always easily related. The time variability of the mass loss phenomenon may explain why it is difficult to relate the properties of CSEs to those of the central stars. Also, some stars may share the same observational properties, but be in slightly different evolutionary stages, with different initial masses and different mass loss histories. It would be extremely useful to get overviews of CSEs that would allow us to smooth the chaotic effects of the mass loss time-variability and as well to measure the total mass expelled by the central stars. With this goal in mind, we are exploring the properties of CSEs around evolved stars by using the atomic hydrogen (H I) line at 21 cm.

Indeed, hydrogen is expected to be the dominant species in stellar winds of evolved stars. It is also expected to be in atomic form right from the stellar atmosphere if the effective temperature, $T_{\rm eff}$, is larger than 2500 K, and to remain atomic in the expanding wind (Glassgold & Huggins 1983). Also, atomic hydrogen should be protected from photoionization by the abundant atomic hydrogen in the interstellar medium (ISM) which absorbs UV photons of energy larger than 13.6 eV. The H I line at 21 cm should thus be an important tracer of stellar winds for late-type stars with $T_{\rm eff} >$ 2500 K, including the outer CSEs where molecules are dissociated. H I studies should bring unique information on the kinematics in these media, and in particular in the regions of interaction with the ISM.

However the detection of red giants in the H I line at 21 cm is hampered by the competing emission from atomic hydrogen in the ISM (which ironically protects the circumstellar atomic hydrogen from destruction) along the same lines of sight. For a long time this difficulty precluded H I observational studies of evolved stars. However, recently, taking advantage of upgraded instruments, we addressed this topic and obtained several detections of AGB stars (Gérard & Le Bertre 2006, Matthews & Reid 2007). In general, a narrow emission line with a quasi-gaussian profile (FWHM $\sim 3\,\mathrm{km\,s^{-1}}$) is observed close to the stellar radial velocity ($V_\star$).

The fate of massive stars is strongly dependent on their mass loss history, which is still poorly understood, in particular when they are red supergiants (van Loon 2010). Our

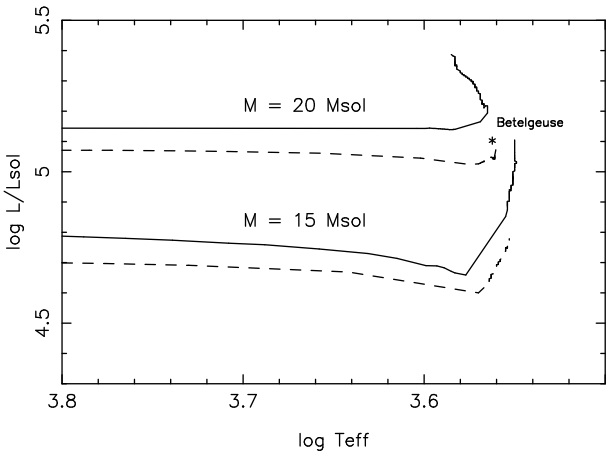

Figure 1. Evolutionary tracks from Meynet & Maeder (2003; Z = 0.02) for stars of initial masses 15 and 20 $M_\odot$ until the end of He-burning; full lines : models with rotation (V_i = 300 km s^{-1}), dashed lines: models without rotation. The star symbol (*) marks the position of α Ori assuming a distance of 200 pc (log $L/L_\odot$= 5.1; T_{eff}= 3650 K).

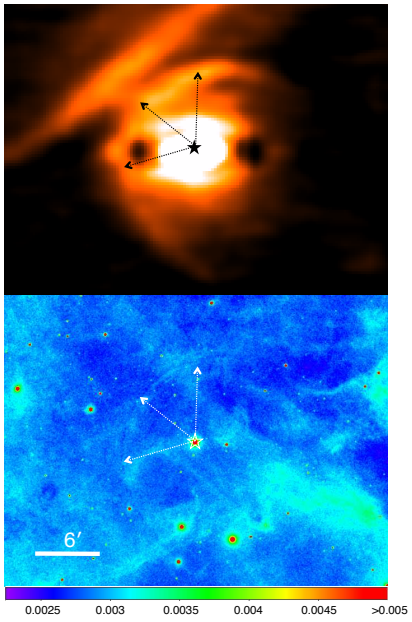

Figure 2. Upper panel: IRAS image at 60 μm centered on α Ori (star symbol). Note the arc (which is pointed by the three arrows), $\sim$6′ north-east of α Ori, and the bar, 10′ north-east (Noriega-Crespo et al. 1997). Lower panel: the same field observed by GALEX. Note the faint narrow counterpart to the 60 μm arc detected by IRAS from PA $\sim$0° to 100°. The scale is in counts per second and per pixel (1.5″).

previous successes encouraged us to extend H I observations to this class of stars. Although suffering from strong galactic H I emission, the supergiant α Ori was detected by Bowers & Knapp (1987) using the Very Large Array. At the position of the star, they found emission from the front and back sides of a CSE expanding at a velocity of 14 km s^{-1}.

In this paper, we report new 21-cm observations of α Ori that we analyze in combination with the previous data from Bowers & Knapp (1987), in order to revisit in H I this otherwise well-documented red supergiant.

2 BASIC DATA

α Ori (Betelgeuse) is the prototype of red supergiants. It has a spectral type M2Iab. Perrin et al. (2004) have measured its effective temperature by infrared interferometry: T_{eff}=3641±53 K. This determination fits well with the revised temperature scale of Galactic Red Supergiants by Levesque et al. (2005, 3650 K for α Ori). It indicates clearly that atomic hydrogen should be the dominant species in the atmosphere and outflow of α Ori.

Although it is the closest supergiant, its distance is not well known. Hipparcos measured a parallax of 7.63±1.64 (Perryman et al. 1997). It has been revised to 6.55±0.83 mas (van Leeuwen 2007), which translates to a distance of 153 pc (135-175 pc). But Harper et al. (2008), using multi-wavelength radio data obtained at the Very Large Array (VLA), derived a smaller parallax/larger distance. When combining the original Hipparcos results with VLA data, they get d=197±45 pc. Harper et al. find also proper motions which are reduced with respect to Hipparcos. They suggest that the Hipparcos parallax is in error because of the large angular size of the star and the motions of the stellar photocenter due to convection (Lim et al. 1998, Haubois et al. 2009, Ohnaka et al. 2011). In the following we follow Harper et al. (2008) and adopt a nominal distance of 200 pc. At this distance, the bolometric luminosity corresponds to log $L/L_\odot \approx 5.10 \pm 0.22$, which, from the Meynet & Maeder (2003) models (see Fig. 1), indicates a progenitor that was an O9V main-sequence star of 20 $M_\odot$ (Harper et al. 2008). Due to mass loss from the main sequence to the red supergiant stage, the present stellar mass would be $\sim$12–16 $M_\odot$. Recently using predictions of limb darkening by stellar atmosphere models and high spatial resolution observations at 1.64 μm, Neilson et al. (2011) estimate a present mass of $11.6^{+5.0}_{-3.9} M_\odot$, in good agreement with Maeder & Meynet's $20 M_\odot$-models. However, this should not be overemphasized since, as mentioned above, the mass loss history of red supergiants is rather insecure.

The proper motions, revised by Harper et al. (2008), are 24.95 mas yr^{-1} in right ascension, and 9.56 mas yr^{-1} in declination. For a distance of 200 pc, and assuming a solar motion, U_0 = 11.1 km s^{-1}, V_0 = 12.24 km s^{-1}, and W_0 = 7.25 km s^{-1} (Schönrich et al. 2010), we derive a velocity in the plane of the sky of 30 km s^{-1} with an apex at PA= 53°.

Like most supergiants, α Ori is surrounded by an extended circumstellar envelope. The physical processes responsible for red supergiant mass-loss are unclear, but may be related to atmospheric convection (Lim et al. 1998, Ohnaka et al. 2011). The convective cells could levitate cool gas above the photosphere and lead to mass loss (Josselin & Plez 2007, Chiavassa et al. 2011). Kervella et al. (2011) have obtained spectacular infrared images with the Very Large Telescope of the European Southern Observatory that show an inhomogeneous spatial distribution of the material ejected by the central star at scales corresponding to several

stellar radii (0.5-3″). IRAS (Infrared Astronomical Satellite) detected an extended structure at 60 μm, which Young et al. (1993a) fitted with a detached shell model of inner radius 0.2′ (0.01 pc at 200 pc) and outer radius 10.5′ (0.6 pc). However, through a careful analysis of high-resolution IRAS data, Noriega-Crespo et al. (1997) discovered a ring ('far-IR arc') of mean radius 6′, mostly confined north-east of α Ori around PA= 60±10°, in good agreement with the apex of the proper motion (Fig. 2). They interpret this structure as a bow shock resulting from the interaction of the supergiant wind with the ISM. Assuming that the IR emission is due to dust, Noriega-Crespo et al. evaluate the mass in the far-IR arc to be ∼ 0.034 $M_\odot$ (at 200 pc). This bow-shock structure was confirmed by Akari at far-infrared wavelengths (Ueta et al. 2008). A straight filament ('bar') is seen at 10′ from the central star ahead of the bow shock. Although perpendicular to the direction of motion and of maximum intensity close to the apex of the bow shock, it does not seem related to α Ori in a simple manner, but may have contributed to the extended emission reported by Young et al. (1993a), which thus appears to be a blend of two distinct sources.

Very recently, α Ori was observed by Herschel at 70 μm and 160 μm (Cox et al. 2012). The images have an unprecedented spatial resolution (6″ and 12″, respectively) and bring many new details that could not be seen on IRAS and Akari images. In particular, they reveal sub-structures in the far-IR arc discovered by IRAS (upper panel of Fig. 2), which breaks up into at least three thin shells. It is also clear that these shells are not circular, and that the radii of curvature, close to apex, are larger than the distance to α Ori, as would be expected from a bow shock. There are also hints of additional arcs at smaller radii.

Finally, our present analysis has uncovered a faint counterpart to this ring in far-ultraviolet (FUV ∼154 nm) imaging obtained by GALEX (Galaxy Evolution Explorer; Martin et al. 2005). The GALEX data presented in Fig. 2 were obtained, from Nov. 29, 2008, to Jan. 14, 2009, as part of the Nearby Galaxies Survey (tile 5786) with an exposure time of 48915 sec. The GR6 pipeline calibrated data were retrieved from the GALEX archive (Morrissey et al. 2007), and smoothed by a Gaussian with kernel width 3 pixels (pixel ≡ 1.5″). The FUV feature is coincident (in projection) with the outer shell revealed by Herschel. It can be seen most clearly north and northeast of the star, although there are hints that the entire structure subtends an angle of at least ∼105° (see arrows on Fig. 2). In the near-UV (∼ 232 nm) the image is unfortunately saturated by a ghost of the central star. A similar, narrow and arc-shaped, UV-feature has been reported around IRC +10216 by Sahai & Chronopoulos (2010). They ascribed the emission to collisionally excited H_2 molecules, although scattering of the interstellar radiation field by small dust particles could as well be considered. On the other hand, the α Ori bar does not seem to be detected by GALEX. To our knowledge the far-UV emission associated with the far-IR arc of α Ori has not been reported before.

The circumstellar envelope of α Ori has also been studied in the CO rotational lines. Huggins (1987) observed a CO(2-1) emission line centered at $V_\star$=3.7±0.4 km s^{-1} (LSR). It implies a 3D space velocity of 31 km s^{-1}, mostly in the plane of the sky. From the profile, Huggins derives an expansion velocity, V_{exp}=14.3 km s^{-1}, and a mass-loss rate of ∼1×10^{-6} $M_\odot$ yr^{-1} (scaled to 200 pc).

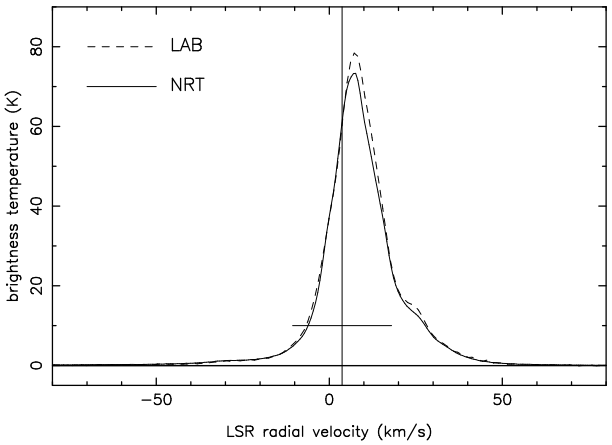

Figure 3. NRT frequency-switched spectrum obtained on the position of α Ori (continuous line) compared to the LAB spectrum (dashed line, Kalberla et al. 2005). We adopted a main beam efficiency of 0.60 for the NRT at 21 cm. The vertical line marks the CO centroid velocity of α Ori and the horizontal bar, the velocity extent of its CO emission (Huggins 1987).

3 NRT SINGLE-DISH OBSERVATIONS

The Nançay Radiotelescope (NRT) is a meridian telescope with a rectangular aperture of effective dimensions 160 m × 30 m. The beam-width at 21 cm is 4′ in right ascension and 22′ in declination. The point source efficiency is 1.4 K Jy^{-1}, and the system noise temperature, 35 K. The observations of α Ori have been obtained in the course of a large survey programme (Gérard et al. 2011) over the period from October 2006 to September 2011.

In Fig. 3, we present a spectrum obtained in the frequency-switched mode of observation. It illustrates that in the direction of α Ori the H I emission is dominated by galactic emission due to interstellar atomic hydrogen along the same line-of-sight. The emission peaks at ∼ 7.5 km s^{-1}. Our spectrum is in good agreement with the spectrum extracted from the Leiden/Bonn/Argentina (LAB) survey (Kalberla et al. 2005; $\phi \sim 36'$). No distinctive feature can be seen in the velocity range expected from the CO observations of α Ori (Huggins 1987).

Data were also obtained in the position-switched mode of observation with the central star placed at the "on-position", and the "off-positions" taken at ±2′, ±4′, and ±6′ in the east-west direction (Fig. 4). These spectra are strongly affected by interstellar confusion. Nevertheless, an emission feature is detected at the radial velocity expected for α Ori (3 km s^{-1}). This is seen in the spectrum with the smallest throw (2′ ≡ 1/2 beam in right ascension, left panel) with a peak intensity of ∼ 0.5 Jy. The intensity is about 1 Jy at ±4′ (1 beam, middle panel) and about 1.2 Jy at ±6′ (1.5 beam, right panel). However, the confusion increases rapidly with throw (see for instance the emission feature at −2 km s^{-1}, and the absorption troughs at +10 and +20 km s^{-1}, that may affect the α Ori line-profiles). We have also obtained spectra with larger throws, but the confusion

becomes so large that the emission feature at 3 $\mathrm{km\,s^{-1}}$ gets drowned.

Finally, position-switched spectra were obtained with the on-positions at $+11'$ (1/2 beam north) and at $-11'$ (1/2 beam south) of the central star. We find that the H I source is centered on the stellar position in declination and that there is no evidence of an extension in the north-south direction (FWHM $\lesssim 11'$).

Despite the high level of confusion, we can infer that an H I source, coincident with α Ori, is detected at $V_{lsr} = 3$ $\mathrm{km\,s^{-1}}$. This source does not appear extended in right ascension as compared to the NRT beam (diameter $\sim 4'$). The line profile is narrow with a FWHM ~ 3 $\mathrm{km\,s^{-1}}$. The integrated intensity is $\approx 5\,\mathrm{Jy \times km\,s^{-1}}$, which translates to ≈ 0.05 $M_\odot$ in atomic hydrogen at 200 pc. This relatively strong emission in H I at a velocity for which Bowers & Knapp (1987) did not report any signal was puzzling and motivated a reassessment of the case at the Very Large Array (VLA).

4 VLA OBSERVATIONS

4.1 C Configuration Observations

Bowers & Knapp (1987) previously observed α Ori in the H I 21-cm line with the VLA of the National Radio Astronomy Observatory (NRAO) in its C configuration (0.08 to 3.2 km baselines).[1] These data comprise 32 frequency channels in a single (right circular) polarization with a channel spacing of 6.10 kHz (1.29 $\mathrm{km\,s^{-1}}$) after on-line Hanning smoothing, resulting in a total bandwidth of 0.189 MHz ($\sim$41 $\mathrm{km\,s^{-1}}$). The band was centered at an LSR velocity of $+5.0$ $\mathrm{km\,s^{-1}}$. In total, $\sim$5.5 hours of integration time was spent on-source. Further details on the observations can be found in Bowers & Knapp (1987).

We downloaded the Bowers & Knapp data from the VLA archive and reprocessed them, following standard procedures for data flagging and gain calibration within the Astronomical Image Processing System (AIPS). The flux densities of our calibration sources are summarized in Table 1. No bandpass calibration was possible owing to contamination of the bandpass calibrator by H I absorption across more than half of the band.

4.2 D Configuration Observations

To obtain improved sensitivity to large-scale H I emission toward α Ori, we obtained additional VLA observations of the star using the VLA D configuration (0.035-1.0 km baselines) over the course of two observing sessions on 2010 January 2-3 (4 hours) and 2010 January 3-4 (6 hours). In total, $\sim$6.7 hours were spent on-source.

The VLA correlator was used in 1A mode with a 1.56 MHz bandpass, yielding 512 spectral channels with 3.05 kHz ($\sim$0.64 $\mathrm{km\,s^{-1}}$) spacing in a single (right circular) polarization. The band was centered at an LSR velocity of 3.7 $\mathrm{km\,s^{-1}}$. Observations of α Ori were interspersed with observations of a phase calibrator, 0632+103, approximately every 20 minutes. 3C48 (0137+331) was used as a flux calibrator, and an additional strong point source (0521+166) was observed as a bandpass calibrator (Table 1). To insure that the absolute flux scale and bandpass calibration were not corrupted by Galactic emission in the band, the flux and bandpass calibrators were each observed twice, with frequency shifts of +1.27 MHz and -1.19 MHz, respectively, relative to the band center used for the observations of α Ori. 0632+103 was also observed once at each of these offset frequencies to permit more accurate bootstrapping of the absolute flux scale to the α Ori data. We estimate that the resulting absolute flux scale has an uncertainty of $\sim$10%.

Data processing was performed using AIPS. At the time of our observations, the VLA contained 21 operational antennas with L-band receivers, 19 of which had been retrofitted as part of the Expanded Very Large Array (EVLA) upgrade. Data obtained during this EVLA transition period require special care during calibration.[2] After applying the latest available corrections to the antenna positions and performing an initial excision of corrupted data, we computed and applied a bandpass calibration to our spectral line data to remove closure errors on VLA-EVLA baselines. The bandpass was normalized using channels 164-447, thus excluding the portion of the band affected by aliasing. We next computed a frequency-averaged (channel 0) data set for use in calibrating the frequency-independent complex gains, again using channels 164-447. Following gain calibration, we applied time-dependent frequency shifts to the data to compensate for changes caused by the Earth's motion during the course of the observations. At this stage, we also applied Hanning smoothing in velocity and discarded every other channel, yielding a 256 channel data set with a velocity resolution of $\sim$1.3 $\mathrm{km\,s^{-1}}$. There were no continuum sources brighter than $\sim$0.02 Jy within our primary beam and none detected within a single spectral channel within $\sim 10'$ of the stellar position, hence no continuum subtraction was performed.

4.3 A Combined VLA Data Set

To obtain a data set with the maximum possible u-v coverage, we have concatenated the VLA C and D configuration data over the velocity range where the two data sets overlap ($-14.3 \geqslant V_{\mathrm{LSR}} \geqslant 24.3$ $\mathrm{km\,s^{-1}}$). This velocity range is sufficient to encompass the range of CO velocities previously observed toward α Ori (see Fig. 3). The u, v, and w values of the C configuration data were precessed to J2000.0 values prior to concatenation.

We imaged the combined data using the AIPS IMAGR program with 'robust +1' weighting of the visibilities. The large-scale Galactic emission along the line-of-sight (Fig. 3) is poorly spatially sampled by the VLA, even in the combined C+D configuration data set, resulting in patterns of strong positive and negative mottling across a number of the channel images. Because such emission cannot be readily deconvolved by standard CLEAN deconvolution algorithms, we performed only a shallow clean (20 iterations) on each spectral channel to reduce sidelobes from strong compact emission features. The rms noise per channel is variable and

[1] The National Radio Astronomy Observatory is operated by Associated Universities, Inc., under cooperative agreement with the National Science Foundation.

[2] See http://www.vla.nrao.edu/astro/guides/evlareturn/.

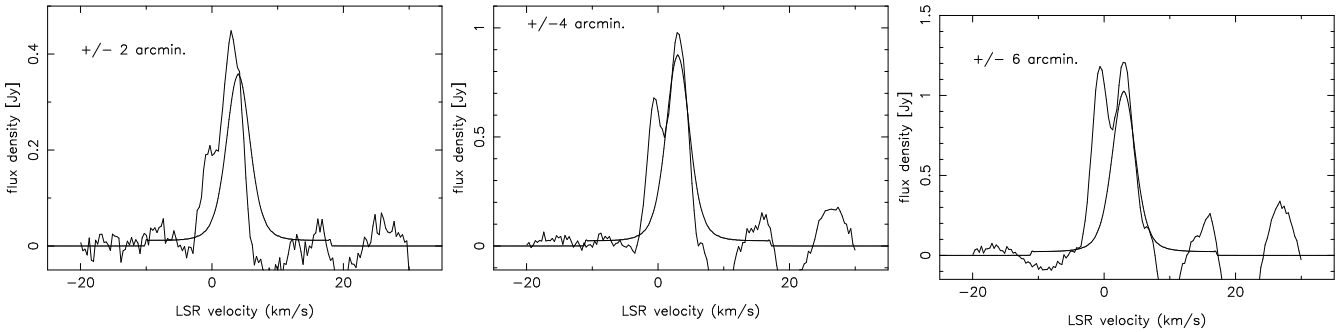

Figure 4. α Ori spectra obtained with the NRT in the position-switched mode. Left: off-positions taken at $\pm 2'$. Centre: off-positions taken at $\pm 4'$. Right: off-positions taken at $\pm 6'$. The thin lines correspond to the modeled spectra discussed in Sect. 5.

Table 1. VLA Calibration Sources

Source	α(J2000.0)	δ(J2000.0)	Flux Density (Jy)	Date
3C48[a]	01 37 41.29	+33 09 35.13	16.038*	1985 Sep 22
...	...	...	15.8778*	2010 Jan 2-4
0521+166[b]	05 21 09.88	16 38 22.05	8.66±0.08†	2010 Jan 2-3
...	...	...	8.40±0.12†	2010 Jan 3-4
0532+075[c]	05 32 38.99	07 32 43.34	2.11±0.01	1985 Sep 22
0632+103[c]	06 32 15.32	10 22 01.67	2.39±0.05†	2010 Jan 2-3
...	...	...	2.25±0.04†	2010 Jan 3-4

Units of right ascension are hours, minutes, and seconds, and units of declination are degrees, arcminutes, and arcseconds.
* Adopted flux density at 1420.76 MHz.
† Mean computed flux density from observations at 1419.57 and 1422.0 MHz; see § 4.
a Primary flux calibrator
b Bandpass calibrator
c Phase calibrator

in most channels is dominated by the complex, large-scale emission.

Despite these complications, we find clear evidence of H I emission associated with α Ori. The channel maps from –11.8 to +23.0 km s^{-1} are presented in Fig. 5. They are strongly affected by extended interstellar emission for velocities above –5 km s^{-1}. Nevertheless an isolated feature coincident with α Ori is clearly seen from −10.5 to −5.3 km s^{-1}. In order to facilitate the identification of small sources, we present in Fig. 6 the channel maps obtained when selecting only the largest u-v spacings ($\geqslant 0.4\,$kλ). The spatial resolution is $\sim 34''$. A source coincident with the central star is detected in the channel maps from –9.2 to –6.6 km s^{-1}, and from +17.9 to +19.2 km s^{-1}. These detections are obtained in channels which correspond approximately to the extreme velocities expected from the wind of α Ori ($V_\star - V_{exp} = -10.6$ km s^{-1}, $V_\star + V_{exp} = 18.0$ km s^{-1}).

We find also emission associated with α Ori at +2.4 km s^{-1} and +3.7 km s^{-1}. Enlarged versions of the two channel maps are shown in Fig. 7 (all baselines) and in Fig. 8 (limited to baselines larger than 0.2 kλ). At +2.4 km s^{-1} (upper panels), the emission peaks on the central star. On the other hand, in the +3.7 km s^{-1} channel map, one notes rather a ring of emission peaks surrounding the position of the star (bottom panels in Figs. 7 and 8). Outside this ring of $\sim 4'$ in size the emission decreases steeply, except south-west where a plateau of emission seems to extend away from the star. The H I emission associated with α Ori in these two channels fits well with that observed at the NRT (Sect. 3).

In addition, the channel maps from +6.3 to +10.1 km s^{-1} (Fig. 6) show H I emission seemingly associated with the arc of far-infrared emission discovered by IRAS $6'$ north-east of α Ori (Noriega-Crespo et al. 1997). Several clumps are also noticeable along the far-IR arc at lower velocities, from –1.5 km s^{-1} to +5 km s^{-1}, and at +10 km s^{-1}. In Fig. 9, the H I emission integrated over the range –1.5 to 8.9 km s^{-1} is overlaid on the IRAS image. The integrated intensity of the H I emission associated with the far-IR arc is ~ 4.9 Jy×km s^{-1}. This is rather uncertain since the structures blend with background emission at low levels and because the maps in Fig. 6 are probably missing some flux. It translates to a mass of $\sim 0.047\,M_\odot$ in atomic hydrogen. Assuming 10% in helium, the total mass can be estimated to be $\sim 0.068\,M_\odot$, which is within a factor 2 of the Noriega-Crespo et al. (1997) estimate for the mass in the far-IR arc. There is perhaps also H I emission at +7.6 km s^{-1} associated with the bar ahead of the arc, but the spatial coincidence is less convincing.

Based on their C configuration data, Bowers & Knapp (1987) reported emission associated with α Ori at ~ -9 km s^{-1} and at $\sim$+17 km s^{-1}, but not at $\sim$+3 km s^{-1}. The reason is that they presented results based only on the largest u-v spacings ($\geqslant 0.4$ kλ). By doing so, they filtered out emission on large scales. As they noted, it is an efficient approach to get rid of most of the confusing interstellar emission. However, excluding the short spacings from the

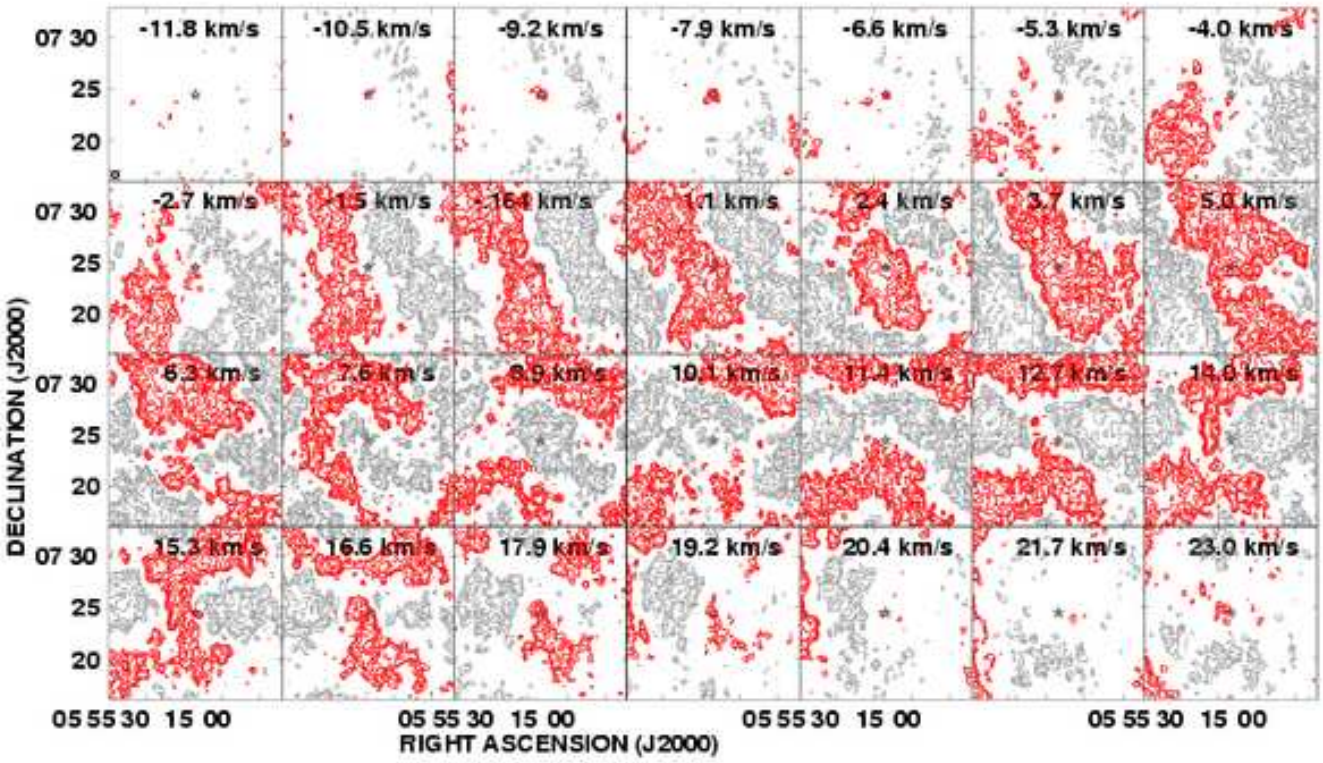

Figure 5. Channel maps obtained at the VLA by combining the data in configuration C of Bowers & Knapp (1987) with our 2010 data in configuration D. The data have a "robust +1" weighting, and the synthesized beam has a size of $37.4'' \times 32.0''$. The contour levels are (-11.2, -8, -5.6, -4, -2.8, -2, 2..., 11.2)×3.9 mJy/beam. The negative contours are in gray, and the positive contours in red. The star symbol marks the position of α Ori.

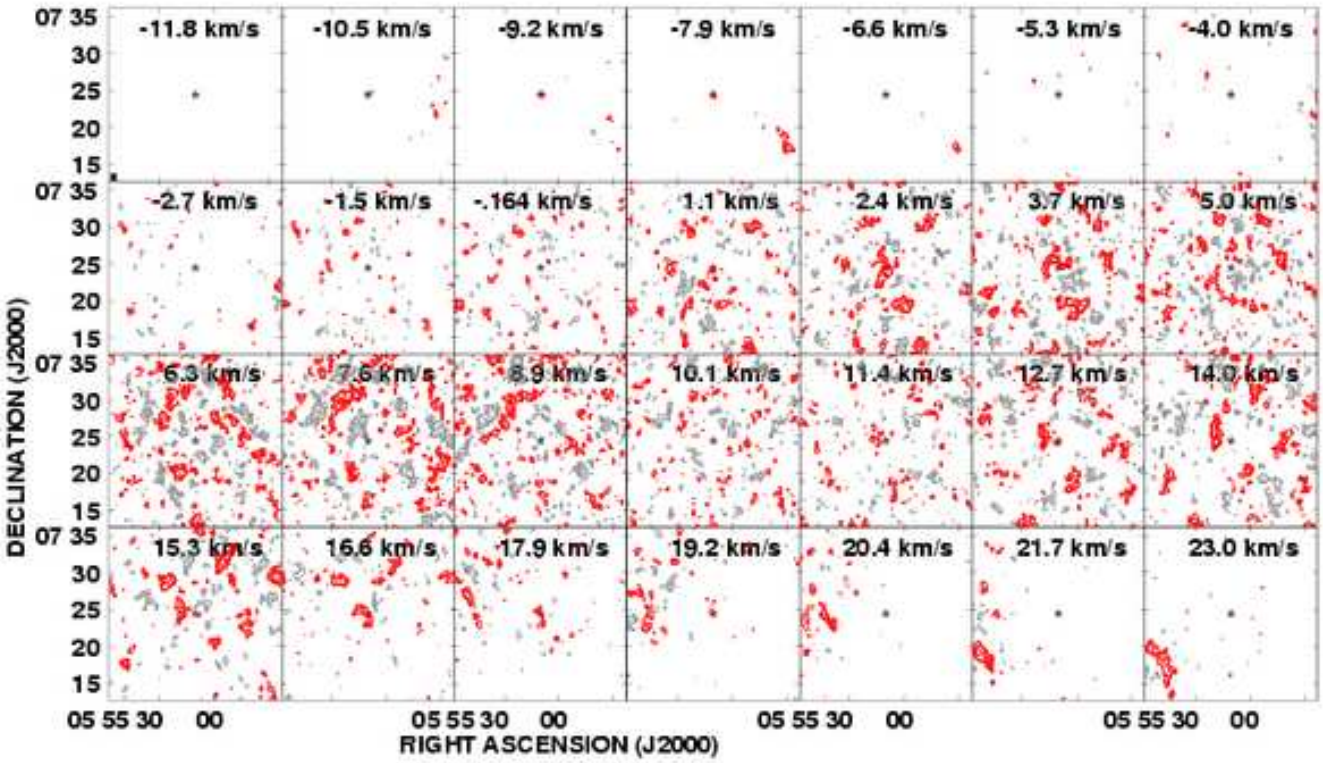

Figure 6. Same as Fig. 5, but selecting baselines larger than 0.4 kλ.

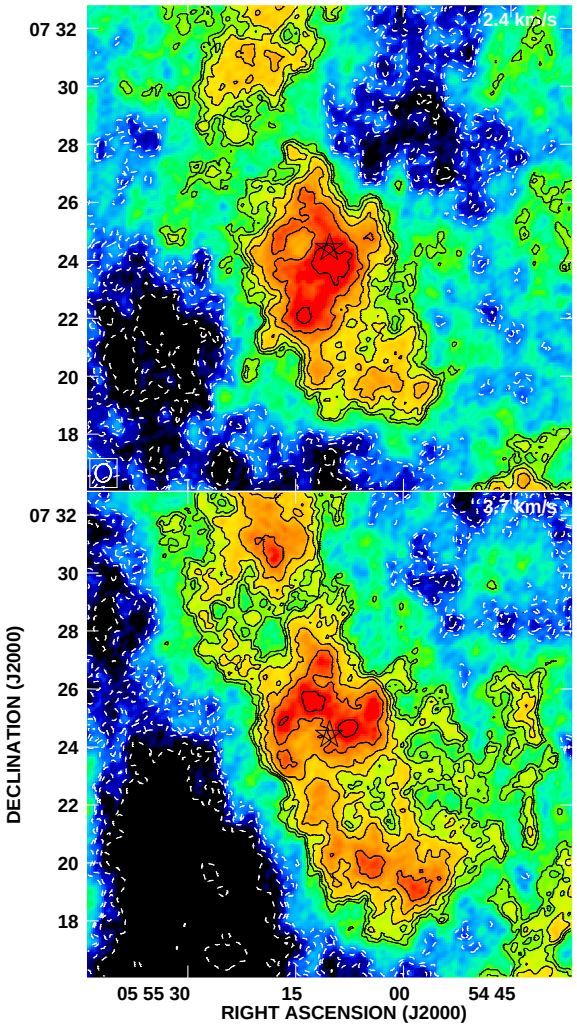

Figure 7. Channel maps at $2.4\,\mathrm{km\,s^{-1}}$ (top) and at $3.7\,\mathrm{km\,s^{-1}}$ (bottom). The star symbol marks the position of α Ori. The contour levels are (-11.2, -8, -5.6, -4, -2, 2,..., 11.2)×3.9 mJy/beam. Dashed lines represent negative contours. Note, in the map at 3.7 $\mathrm{km\,s^{-1}}$, the emission peaks that surround the central star and appear to define the α Ori gas detached shell.

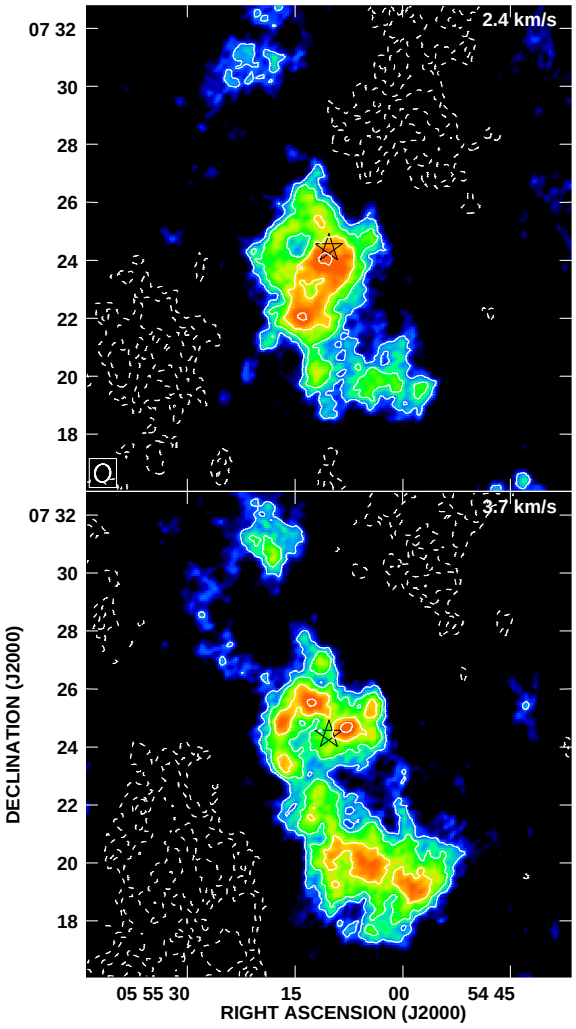

Figure 8. Same as Fig. 7, but restricted to baselines larger than 0.2 kλ. The contour levels here are (-8, -5.6, -4, 4, 5.6, 8, 11.2)×3.9 mJy/beam.

C-configuration data removes also all signatures of the shell. In particular for α Ori at $\sim$+3 $\mathrm{km\,s^{-1}}$, it removed the source of $\sim 4'$ in size associated with α Ori which was detected by the NRT. If the same filtering is applied to the merged C+D data, only the ring of emission peaks is left, as can be seen in the 3.7 $\mathrm{km\,s^{-1}}$ channel map of Fig. 6.

Conversely, when we isolate the data obtained in configuration D, we only detect unambiguously a point source around –8 $\mathrm{km\,s^{-1}}$. The channel maps at LSR velocities larger than –5 $\mathrm{km\,s^{-1}}$ suffer heavily from interstellar emission. In spite of this confusion, a source is detected at +3 $\mathrm{km\,s^{-1}}$, but it does not show the complex structure visible in Fig. 7 because of the lower spatial resolution. Also a peak of emission is visible around +17 $\mathrm{km\,s^{-1}}$, but it is immersed in a larger structure. The combination of data obtained in configurations C and D is thus essential to reveal the full range of features that have been described above.

5 INTERPRETATION

A star which is undergoing mass loss gets progressively surrounded by an expanding circumstellar shell. However, the collision of the supersonic stellar wind with the surrounding medium (ISM or an older envelope) produces a shell of denser material that is slowly expanding (Lamers & Cassinelli 1999). "Detached shells" have been reported to be detected by IRAS around many evolved stars (Young et al. 1993a). The emission of the detached shells observed at 60 and 100 μm is commonly assumed to be continuum emission radiated thermally by dust (Kerschbaum et al. 2010). Young et al. (1993b) developed a model of a dust shell expanding into the ISM that simulates the formation of a detached shell and accounts for the IRAS results.

The Young et al. (1993b) scenario was revived by Libert et al. (2007) who developed a spherical model adapted to the gas and to the modeling of its H I line emission. In this model a detached shell is produced by a stellar outflow that is abruptly slowed down at a termination shock. This first shock defines the inner limit of the detached shell (r_1).

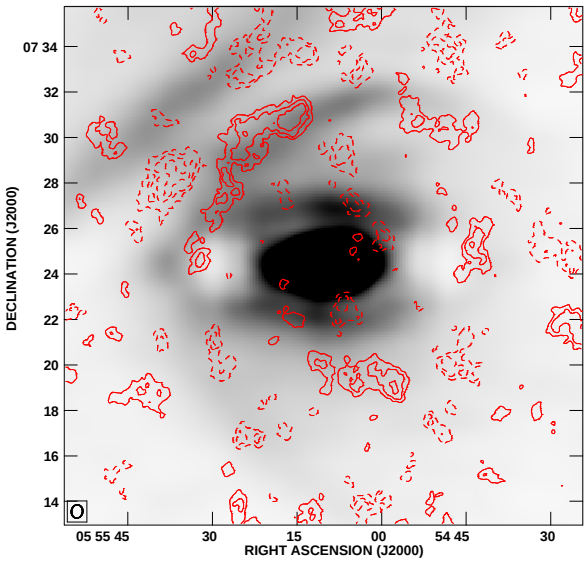

Figure 9. H I emission from Fig. 6, summed from -1.5 to 8.9 km/s. The contour levels are (-8., -5.6, -4., -2.8, 2.8, 4., 5.6, 8.)×1.8 mJy/beam. The background image is from IRAS (see Fig. 2). Note the association between H I emission and the far-IR arc.

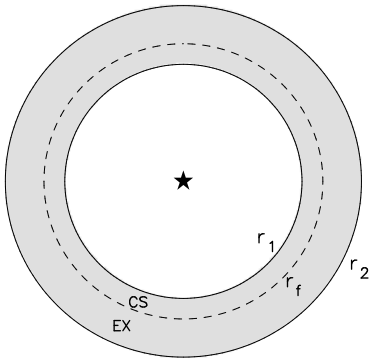

Figure 10. Schematic view of the α Ori detached shell. The termination shock is located in r_1, the contact discontinuity in r_f, and the bow shock in r_2. CS stands for circumstellar material and EX, for external material.

The outer limit (r_2) is defined by the leading shock (bow shock) where external matter is compressed by the expanding shell (Fig. 10). Between these two limits, the detached shell is composed of compressed circumstellar matter and interstellar matter separated by a contact discontinuity at r_f. The circumstellar matter is decelerated and heated when crossing the shock in r_1. As it cools down from T_1^+ (in r_1) to T_f (in r_f), the expansion velocity decreases further, from v_1^+ to v_f, and the density increases from n_1^+ to n_f^-. Adopting an arbitrary temperature profile, Libert et al. (2007) solve numerically the equation of motion between r_1 and r_f. The temperature profile in the detached shell is constrained by the observed H I line profiles. For the external part of the detached shell (between r_f and r_2), Libert et al. (2007) assume a density profile that falls off as $1/r^2$ with the condition that the total mass ($M_{DT,CS}$) is given by the equivalent ISM mass enclosed in a sphere of radius r_2. Inside r_1, Libert et al. assume a spherical wind in uniform expansion.

Originally Libert et al. (2007) developed this model for Y CVn, a carbon star surrounded by a dust detached shell discovered by IRAS (Young et al. 1993a) and imaged by ISO (Izumiura et al. 1996). H I line profiles obtained at different positions on and around the central star were well fitted by such a model with a gas temperature decreasing from 1800 K, in r_1, to 170 K, in r_f. Libert et al. applied the same model to other sources, like RX Lep, an oxygen-rich star (Libert et al. 2008), and V1942 Sgr, another carbon star (Libert et al. 2010). In general, the gas detached shell model of Libert et al. (2007) accounts well for the H I emission of evolved stars, which are characterized by a narrow line profile ($\sim$ 2-4 km s^{-1}) approximately centered on the stellar radial velocity (Gérard & Le Bertre 2006). Indeed the emission from the detached shell where matter has been accumulating generally dominates the emission from the freely expanding wind region inside r_1. The H I emission from an unresolved spherical wind would be characterized by a rectangular line profile of width twice the expansion velocity (Gardan et al. 2006).

However, at high spatial resolution, the inner region ($< r_1$) may be resolved. In such a case a spectrum obtained on the stellar position should show two horns separated by twice the expansion velocity. In addition, a central line, corresponding to the detached shell should be observed in the middle, at the stellar radial velocity. Thus, for mass losing evolved stars, the Libert et al. (2007) model predicts a characteristic three-peaked profile at the central position, and a single-line profile away from it ($> r_1$) with a maximum intensity close to the inner shell boundary.

The merged VLA data show two peaks of emission centered on α Ori at $V_\star \pm V_{exp}$. Close to $V_\star$, one notes also a peak on the star (Fig. 7, upper panel) and a ring of emission around the star (Fig. 7, lower panel). Fig. 11 shows spectra that have been extracted from the VLA merged data set at the position of the star and in a ring of internal radius, 80″, and external radius, 160″. We expect that such a ring encloses most of the H I emission from the detached shell. In the upper panel of Fig. 11, the predicted three-peaked profile is seen, with the peaks close to the expected velocities. On the other hand a single peak at $V_\star$ is visible in the spectrum shown in the lower panel. It thus seems that the VLA data contain information which, at least qualitatively, agrees with the Libert et al. (2007) model. However, the emission intrinsic to α Ori is partly hidden by the confusion due to the ISM emission, as evidenced by the negative peaks at 9 km s^{-1}. Similarly, the NRT data show an emission feature centered close to $V_\star$. Due to its large beam, the NRT cannot detect the emission from the free-flowing wind of α Ori.

In view of these results, we have run the Libert et al. (2007) model with parameters (distance, expansion velocity, etc.) that apply to α Ori (see Sect. 2). As the stellar effective temperature is larger than 2500 K, we assume that all hydrogen is in atomic form (Glassgold & Huggins 1983). We assume also that 90% of the mass is in hydrogen and 10% in helium, so that the mean molecular weight, μ, is equal to 1.3. An expansion velocity of the free wind, $v_0 = 14$ km s^{-1}, implies a post-shock temperature in r_1 of almost 5800 K (see Table 2). For the internal radius we select

a value of 2′ (≡0.12 pc) in order to get a maximum H I intensity at a position corresponding to the emission peaks identified in Fig. 7. The external radius was set arbitrarily to r_2=3′, and the ISM density to n_H=1 cm^{-3}. The calculated H I emission is convolved with the telescope beam profile. For the NRT, we adopt the response of a rectangular aperture of 160 m×30 m (Gardan et al. 2006), and for the VLA a Gaussian response of FWHM = 34″.

We have tried several combinations of mass-loss rate and duration of the mass loss episode. The mass-loss rate is constrained by the intensity of the peaks observed at $V_\star \pm V_{exp}$ (i.e. –10 and +18 km s^{-1}) on the star. The mass in atomic hydrogen in the detached shell (which can be estimated by the emission feature observed at $V_\star$) constrains the product of the mass loss rate by the duration. We found satisfactory fits for values of $\dot{M}$ in the range 1.0 to 1.5×10^{-6} M$_\odot$ yr^{-1} and values of the duration in the range 0.7 to 1.0×10^5 years.

In Figs. 4 and 11 we present the results of our best compromise that was obtained with $\dot{M} = 1.2\times10^{-6}$ M$_\odot$ yr^{-1} and a total duration of 0.8×10^5 years. The parameters corresponding to this preferred model are summarized in Table 2. A rapid cooling of the gas (with a temperature assumed to vary as a power law from 5800 K in r_1 to 220 K in r_f) is needed in order to reproduce the observed narrow line width (∼ 3 km s^{-1}) of the emission coming from the detached shell.

In this spherical modeling we have adopted a systemic radial velocity of 3 km s^{-1}, which gives the best agreement with NRT data. The H I emission from AGB stars is known to be sometimes shifted by ∼1–3 km s^{-1} with respect to the CO emission which is believed to provide the most precise estimate of the stellar radial velocity (Gérard & Le Bertre 2006). In general this shift is towards 0 km s^{-1} (LSR), probably an effect of the dragging of the circumstellar shell by the ambient ISM. In Fig. 11 (upper panel) it is clear that the central peak is not centered at the average of the two horn velocities. Consistently the model predicts horns that are blueshifted by ∼ 1 km s^{-1}.

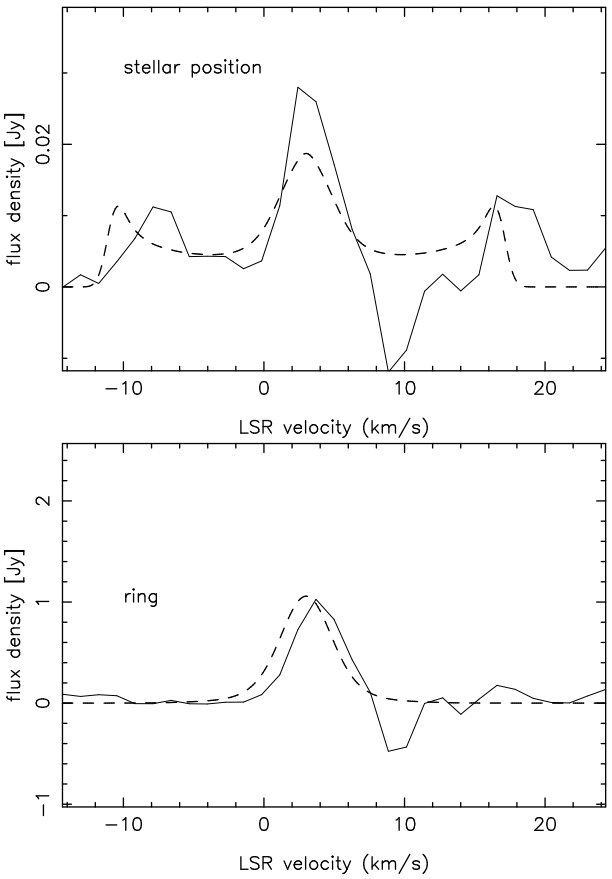

Figure 11. Upper panel: H I profile obtained on α Ori with the VLA within an aperture of 34″ diameter. Lower panel: H I profile obtained by integrating the emission within a ring of internal radius, 80″, and external radius, 160″, and centered on the star. The dashed lines correspond to the modeled spectra discussed in Sect. 5.

Table 2. Model parameters (d = 200 pc). The notations are as in Libert et al. (2007). In particular, t_{DS} is the formation time of the detached shell, $M_{DT,CS}$ is the mass of the circumstellar component of the detached shell, and $M_{DT,EX}$ is the external mass accreted in the detached shell.

$\dot{M}$	1.2×10^{-6} M$_\odot$ yr^{-1}
μ	1.3
t_1	8 140 years
t_{DS}	71 860 years
r_1	0.12 pc (2.0′)
r_f	0.14 pc (2.35′)
r_2	0.18 pc (3.0′)
$T_0(\equiv T_1^-)$, T_1^+	20 K, 5796 K
T_f (= T_2)	223 K
$v_0(\equiv v_1^-)$, v_1^+	14 km s^{-1}, 3.51 km s^{-1}
v_f	0.06 km s^{-1}
v_2	0.9 km s^{-1}
n_1^-, n_1^+	14.0 H cm^{-3}, 55.8 H cm^{-3}
n_f^-, n_f^+	1.8×10^3 H cm^{-3}, 2.5 H cm^{-3}
n_2	1.6 H cm^{-3}
$M_{r<r_1}$	9.8×10^{-3} M$_\odot$
$M_{DT,CS}$	0.086 M$_\odot$
$M_{DT,EX}$	0.8×10^{-3} M$_\odot$

6 DISCUSSION

With the NRT and the VLA, we have detected an H I source coincident with α Ori and relatively compact (∼ 4′ in right ascension). The emission is centered at V_{lsr}∼ 3 km s^{-1}, and has a narrow line profile (FWHM ∼ 3 km s^{-1}). In addition, the VLA channel map at 3.7 km s^{-1} shows a ring of emission encircling the position of the star and a tail extending southwest. Furthermore, the VLA data show emission lines at −9 km s^{-1} and at +18 km s^{-1}, right at the position of the central star. Although our data are affected by confusion, these features can be clearly ascribed to the circumstellar shell expelled by the supergiant.

These features can be explained qualitatively by the Libert et al. (2007) detached shell model. In particular, the spectrally narrow emission observed close to $V_\star$, which the VLA shows to peak along a ring encircling the position of α Ori at 3.7 km s^{-1}, is characteristic of the emission expected from a detached shell. Using parameters which are representative of α Ori, the model gives a fair agreement with the observations. The main result is that the detached gas shell

of α Ori can be accounted for by a mass loss episode of $\sim 10^5$ years duration at a rate in the range 1-2$\times 10^{-6}$ $M_\odot\,yr^{-1}$.

In Sect. 4.3, we noted that Bowers & Knapp (1987) detected only the horns at $V_\star \pm V_{exp}$ corresponding to the free flowing wind of α Ori, because they had selected large *u-v* spacings. They modeled these horns with a wind of 2.2×10^{-6} $M_\odot\,yr^{-1}$ (at 200 pc). In fact this agrees quite well with our model, because they adopted an envelope radius of $60''$, half as much as our own r_1 estimate. The reprocessing of their full data set and the combination with D-configuration data revealed the stationary shell of size $\sim 4'$ that they missed.

Here we want to stress again the importance of multi-scale observations, and in particular of the C-configuration data that we have retrieved from the VLA archive. Indeed, it is the improved angular resolution that allows us to characterize geometrically the detached shell. For three other sources that we have studied with the VLA in configuration D, Mira (Matthews et al. 2008), RS Cnc (Matthews & Reid 2007, Libert et al. 2010) and X Her (Matthews et al. 2011), we have not observed shells that are seen to be detached from the central stars. However the observed H I line-profiles indicate that the stellar winds are slowed down by the external medium, and that the outer circumstellar shells should be quasi-stationary with an enhanced density. Thus we expect that observations of these sources with a higher spatial resolution would reveal a detachment of the outer shells.

The mass-loss rate that we find is smaller than the mass-loss rate used by Meynet & Maeder (2003) in the evolution of a 20-$M_\odot$ star which, among their models, gives the best agreement with the temperature and luminosity of α Ori. A better agreement on the temperature and mass-loss rate might be found for models with a lower initial mass of α Ori, but also with a lower luminosity, which would imply a distance lower than 150 pc. We note however that, for the mass loss of cool stars, Meynet & Maeder (2003) use prescriptions from de Jager et al. (1988), which produce in their models smooth variations of the mass-loss rate with time. This is only indicative, as mass loss is known to be strongly variable in the progenitors of red supergiants, especially when they cross the instability strip.

From observations, the mass-loss rate of α Ori is uncertain, and values ranging over a factor 10 have appeared in the literature. For instance De Beck et al. (2010), from a modeling of several CO rotational lines, derive a mass loss rate of $\sim 5 \times 10^{-7}$ $M_\odot\,yr^{-1}$ (for a distance of 200 pc), whereas Harper et al. (2001, 2009), from a model of the radio continuum emission, obtained 4.8 ($\pm$1.3)$\times 10^{-6}$ $M_\odot\,yr^{-1}$ (for the same distance). This large range arises in part from tracers probing different regions of the circumstellar shell, and from a rate of mass loss that has likely been variable. Also the CO emission seems anomalously low in red supergiants which could lead to an underestimate of the mass-loss rate (Josselin et al. 1998). Interferometric data obtained at 11 μm by Danchi et al. (1994) seem to show the presence of several dust shells close (at 1 and $2''$) to the central star, suggesting a mass loss rate that is highly variable. We have adopted a value (1.2×10^{-6} $M_\odot\,yr^{-1}$) which, in our model, represents an average over 8000 years.

In our modeling the gas temperature decreases from 5800 K (in r_1) to 220 K (in r_f) in a lapse of 72×10^3 years. This translates to an average cooling time-scale of 2.2×10^4 years. The post-shock density is 56 H cm^{-3}, and rises up to 1800 H cm^{-3} at the contact discontinuity. Spitzer (1968) gives a cooling time of about 2.5×10^4 years for a gas of density 10 H cm^{-3} and temperature 1000 K. Therefore the modeling is consistent with a quite reasonable hypothesis for the cooling. The cooling per unit mass is proportional to the density. From Dalgarno & McCray (1972) it should also depend on the electron density and on the temperature. From our modelling we can estimate the temperature and the density as a function of the distance to the central star. The electron density is an unknown. However, hydrogen should stay atomic within the detached shell, but species with a low ionization potential, such as carbon, are expected to be singly ionized (Huggins et al. 1994).

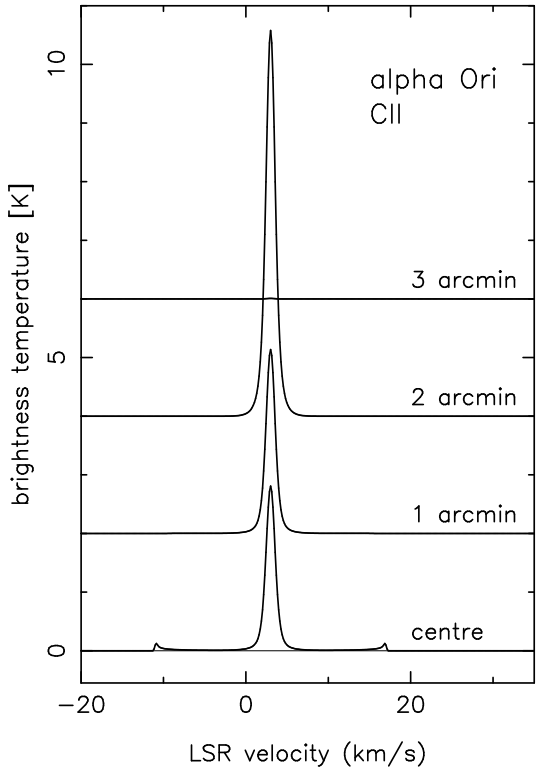

Figure 12. Simulation of the C II line emission at various distances from α Ori. For clarity, the spectra are successively shifted by 2 K.

The cooling lines from the detached shell are predicted to be centered at the same velocity as the H I line (3 km s^{-1}), and to have a similarly narrow line-profile ($\sim$3 km s^{-1}). As an example we give the profile of the C II line at 158 μm at various positions across the detached shell (Fig. 12). We assumed carbon to have an abundance of 2×10^{-4} relative to hydrogen and to be completely ionized beyond 6×10^{-3} pc ($0.1'$) from the central star. The calculation has been done assuming a gaussian beam of $12''$ (FWHM), and adopting the same temperature profile as for hydrogen (Sect. 5). This cooling line should be within reach of the IR Heterodyne Spectrometer on the SOFIA (Stratospheric Observatory for Infrared Astronomy).

The efficient cooling that we have adopted implies that the detached gas shell in the model is geometrically narrow ($r_f/r_1 \sim 1.2$). This could be an explanation for the relative compactness of the H I source ($\phi \sim 4'$) and for the squeezing

of the contours around the central star (except south-west) in the 2.4 and 3.7 $\mathrm{km\,s^{-1}}$ channel maps (Figs. 7 and 8).

The model that we are using is spherical and cannot account for all the features observed in α Ori , which is known to be moving through the ISM at $\sim 30\,\mathrm{km\,s^{-1}}$ towards the north-east. The plateau that is observed south-west in the 3.7 $\mathrm{km\,s^{-1}}$ channel map could be the signature of a tail of material such as that observed behind Mira (Matthews et al. 2008). This kind of feature is predicted by 3D hydrodynamic simulations of CSEs around mass losing stars moving through the ISM, such as those performed by Villaver et al. (2003) or by Wareing et al. (2007), and might hopefully contain information on past episodes of mass loss.

The H I emission that we observe in α Ori is concentrated in a source of diameter $\sim 4'$, and is thus found well inside the infrared emission reported by Noriega-Crespo et al. (1997) and by Ueta et al. (2008), and that Herschel has shown to arise from several thin shells of radii $\sim 6'$ (Cox et al. 2012). These shells are clearly distinct from the classical detached shells of Young et al. (1993a). The mechanism responsible for the far-infrared emission of these shells has not been identified with certainty. It could be emission by dust heated by collisions with the shocked gas and/or emission from forbidden lines of O I and C II. However there is a consensus that this emission traces the bow shock(s) resulting from the motion of α Ori through the ISM. van Marle et al. (2011) have studied the coupling of dust and gas within a shocked wind with conditions typical of α Ori. They find that, apart for large grains (radius $> 0.045\,\mu$m), the dust remains bound to the gas in such a structure.

We found however that the far-IR arc coincides with FUV emission and is associated with atomic hydrogen emission (Figs. 6 and 9). The mass in atomic hydrogen compares fairly well with the estimate of the total mass of the far-IR arc by Noriega-Crespo et al. (1997), given the uncertainties in our H I estimate and in the gas-to-dust ratio (100) adopted by Noriega-Crespo et al. H I emission is found mainly at 7.6 ± 1.3 $\mathrm{km\,s^{-1}}$, i.e. at the velocity at which interstellar emission peaks (see Fig. 3). Thus the atomic gas that we detect in coincidence with the far-IR arc seems related to the surrounding ISM rather than to α Ori. Possibly, it is interstellar matter compressed in a precursor ahead of the bow shock.

The ISM gas that crosses the bow shock at $\sim 30\,\mathrm{km\,s^{-1}}$ should be heated at a temperature $\sim 25\,000$ K, and hydrogen may be ionized. Except to the south-west, we have found no unambiguous evidence of atomic hydrogen associated with α Ori beyond $3'$ from the star. This suggests that hydrogen in the region between the interface and the bow shock remains ionized during the lapse of $\sim 10^5$ years that we infer for the formation of the detached shell, or that it remains sufficiently warm that its emission is widened over a large range of velocities, preventing its detection. In these conditions, our H I modeling cannot bring real constraints on the region of the detached shell which is filled by matter from the ISM. In particular, the value that we have adopted for the parameter r_2 has no real significance.

Conversely, the parameters that we find for the circumstellar part of the detached shell could be used as constraints for the 3D hydrodynamic simulations of the Betelgeuse's bow shock that start to be developed (e.g. Mohamed et al. 2011). In this specific case, we note that the interface is at $\gtrsim 0.3$ pc from the central star, which seems too large compared to our H I observations, that suggest a smaller value. Possibly the rate of mass loss adopted by Mohamed et al. ($3\times10^{-6}\,\mathrm{M_\odot\,yr^{-1}}$) is too large. The density of the ISM material through which α Ori is moving is also uncertain.

Another possibility is that the far-IR arc seen at $6'$ from α Ori is not the true bow shock related to the detached gas shell that is detected at 21 cm. The examination of the images published by Cox et al. (2012) suggests that there are other structures inside the far-IR arc, in particular another arc at $3'$ north-east of α Ori. It is tempting to hypothesize that this $3'$-radius arc is the true bow shock related to the detached shell that we have modeled. In that case the $6'$-radius arc which is also seen in H I and far-UV would be related to a more ancient episode of mass loss. Clearly spectral information on the far-IR emission of this arc and imaging in H I at a higher spatial resolution are needed in order to elaborate on its true nature. The characteristics of the internal medium, between the detached shell and the far-IR arc, are also an issue.

7 CONCLUSIONS

Observations in the H I line at 21 cm of α Ori have been performed with the NRT and the VLA. A source ($\phi \sim 4'$) has been detected at the position of the star. The emission is dominated by a narrow line (FWHM ~ 3 $\mathrm{km\,s^{-1}}$) centered close to $V_\star$. The VLA data show that this source has the structure of a detached shell elongated towards the south-west. This shape agrees with the numerical simulations of a CSE moving through the ISM. Emission peaks at $V_\star \pm V_{\rm exp}$ are also observed by the VLA at the position of the central star. Presently the data bring no clear evidence of atomic hydrogen outside this source.

We have developed a working model adapted to α Ori and its detached neutral gas shell that accounts for the spectral features that are observed and for the size of the source. In this model, the detached gas shell of α Ori results from the collision of a 1.2×10^{-6} $\mathrm{M_\odot\,yr^{-1}}$ stellar wind, expanding at $14\,\mathrm{km\,s^{-1}}$, with the surrounding ISM for a lapse of $\sim 10^5$ years. The gas is cooling from a post-termination-shock temperature of 5800 K to $\sim$220 K, at the interface with ISM.

The high level of confusion in the direction of α Ori forces us to be cautious. Nevertheless, by selecting different ranges of baselines, it is possible to obtain images revealing the detached shell of α Ori as well as H I emission coincident with the $6'$ far-IR/far-UV arc. Presently, we cannot conclude on the exact nature of the structure in arc discovered by IRAS. We suggest that the H I emission might come from a precursor of the α Ori bow shock, or that the whole structure could be related to an ancient episode of mass loss.

ACKNOWLEDGMENTS

The Nançay Radio Observatory is the Unité scientifique de Nançay of the Observatoire de Paris, associated as Unité de Service et de Recherche (USR) No. B704 to the French Centre National de la Recherche Scientifique (CNRS). The

Nançay Observatory also gratefully acknowledges the financial support of the Conseil Régional de la Région Centre in France. The VLA observations presented here are part of the NRAO program AM1001. LDM acknowledges support from grant AST-1009644 from the National Science Foundation. This research has made use of the SIMBAD and ADS databases. We thank Dr. Graham Harper for his careful reading of the manuscript and useful comments.

REFERENCES

Bowers, P. F., & Knapp, G. R., 1987, ApJ, 315, 305
Bowers, P. F., & Knapp, G. R., 1988, ApJ, 332, 299
Chiavassa, A., Haubois, X., Young, J. S., Plez, B., Josselin, E., Perrin, G., & Freytag, B., 2011, A&A, 515, A12
Cox, N. L. J., Kerschbaum, F., van Marle, A.-J., et al., 2012, A&A, 537, A35
Dalgarno, A., & McCray, R. A., 1972, ARAA, 10, 375
Danchi, W. C., Bester, M., Degiacomi, C. G., Greenhill, L. J., & Townes, C. H., 1994, AJ, 107, 1469
De Beck, E., Decin, L., de Koter, A., et al., 2010, A&A, 523, A18
de Jager, C., Nieuwenhuijzen, H., & van der Hucht, K. A., 1988, A&AS, 72, 259
Gardan, E., Gérard, E., & Le Bertre, T., 2006, MNRAS, 365, 245
Gérard, E., & Le Bertre, T., 2006, AJ, 132, 2566
Gérard, E., Le Bertre, T., & Libert, Y., 2011, Proc. "*SF2A 2011*", G. Alecian, K. Belkacem, S. Collin, R. Samadi & D. Valls-Gabaud (eds.), p. 419
Glassgold, A. E., & Huggins, P. J., 1983, MNRAS, 203, 517
Harper, G. M., Brown, A., & Guinan, E. F., 2008, AJ, 135, 1430
Harper, G. M., Brown, A., & Lim, J., 2001, ApJ, 551, 1073
Harper, G. M., Richter, M. J., Ryde, N., Brown, A., Brown, J., Greathouse, T. K., & Strong, S., 2009, ApJ, 701, 1464
Haubois, X., Perrin, G., Lacour, S., et al., 2009, A&A, 508, 923
Huggins, P. J., 1987, ApJ, 313, 400
Huggins, P. J., Bachiller, R., Cox, P., & Forveille, T., 1994, ApJ, 424, L127
Izumiura, H., Hashimoto, O., Kawara, K., Yamamura, I., & Waters, L. B. F. M., 1996, A&A, 315, L221
Josselin, E., Loup, C., Omont, A., Barnbaum, C., Nyman, L.-Å., & Sèvre, F., 1998, A&AS, 129, 45
Josselin, E., & Plez, B., 2007, A&A, 469, 671
Kalberla, P. M. W., Burton, W. B., Hartmann, D., Arnal, E. M., Bajaja, E., Morras, R., & Pöppel, W. G. L., 2005, A&A, 440, 775
Kerschbaum, F., Ladjal, D., Ottensamer, R., et al., 2010, A&A, 518, L140
Kervella, P., Perrin, G., Chiavassa, A., Ridgway, S. T., Cami, J., Haubois, X., & Verhoelst, T., 2011, A&A, 531, A117
Lamers, J. G. L. M., & Cassinelli, J. P., 1999, "Introduction to Stellar Winds", Cambridge University Press, Chap. 12
Levesque, E. M., Massey, P., Olsen, K. A. G., et al., 2005, ApJ, 628, 973
Libert, Y., Gérard, E., & Le Bertre, T., 2007, MNRAS, 380, 1161
Libert, Y., Gérard, E., Thum, C., Winters, J. M., Matthews, L. D., & Le Bertre, T., 2010, A&A, 510, A14
Libert, Y., Le Bertre, T., Gérard, E., & Winters, J. M., 2008, A&A, 491, 789
Libert, Y., Winters, J. M., Le Bertre, T., Gérard, E., & Matthews, L. D., 2010, A&A, 515, A112
Lim, J., Carilli, C. L., White, S. M., Beasley, A. J., & Marson, R. G., 1998, Nature, 392, 575
Martin, D. C., Fanson, J., Schiminovich, D., et al., 2005, ApJ, 619, L1
Matthews, L. D., Libert, Y., Gérard, E., Le Bertre, T., Johnson, M. C., Dame, T. M., 2011, AJ, 141, id. 60
Matthews, L. D., Libert, Y., Gérard, E., Le Bertre, T., & Reid, M. J., 2008, ApJ, 684, 603
Matthews, L. D., & Reid, M. J., 2007, AJ, 133, 2291
Meynet, G., & Maeder, A., 2003, A&A, 404, 975
Mohamed, S., Mackey, J., & Langer, N., 2011, A&A, in press (arXiv:1109.1555)
Morrissey, P., Conrow, T., Barlow, T. A., et al., 2007, ApJS, 173, 682
Neilson, H. R., Lester, J. B., & Haubois, X., 2011, to appear in the proceedings of "The 9$^{\rm th}$ Pacific Rim Conference on Stellar Astrophysics", ASP Conf. Ser. (arXiv1109.4562)
Noriega-Crespo, A., van Buren, D., Cao, Y., & Dgani, R., 1997, AJ, 114, 837
Ohnaka, K., Weigelt, G., Millour, F., et al., 2011, A&A, 529, A163
Perrin, G., Ridgway, S. T., Coudé du Foresto, V., Mennesson, B., Traub, W. A., & Lacasse, M. G., 2004, A&A, 418, 675
Perryman, M. A. C., Lindegren, L., Kovalevsky, J., et al., 1997, A&A, 323, L49
Sahai, R., & Chronopoulos, C. K., 2010, ApJ, 711, L53
Schönrich, R., Binney, J., & Dehnen, W., 2010, MNRAS, 403, 1829
Spitzer, L., 1968, "Diffuse Matter in Space", Interscience Publishers, p. 139
Ueta, T., Izumiura, H., Yamamura, I., et al., 2008, PASJ, 60, S407
van Leeuwen, F., 2007, "Hipparcos, the New Reduction of the Raw Data", Springer, Astrophysics and Space Science Library, vol. 350
van Loon, J. T., 2010, ASP Conf. Ser., 425, 279
van Marle, A. J., Meliani, Z., Keppens, R., & Decin, L., 2011, ApJ, 734, L26
Villaver, E., García-Segura, G., & Manchado, A., 2003, ApJ, 585, L49
Wareing, C. J., Zijlstra, A. A., & O'Brien, T. J., 2007, MNRAS, 382, 1233
Young, K., Phillips, T. G., & Knapp, G. R., 1993a, ApJS, 86, 517
Young, K., Phillips, T. G., & Knapp, G. R., 1993b, ApJ, 409, 725